

**Acoustics'08  
Paris**  
June 29-July 4, 2008

[www.acoustics08-paris.org](http://www.acoustics08-paris.org)

## **A multistatic synthetic aperture sonar to detect a cylinder lying on a rough interface: experimental results**

Caroline Herve<sup>a</sup>, Jean-Pierre Sessarego<sup>a</sup>, Régine Guillermin<sup>a</sup>, Françoise Schmitt<sup>b</sup> and Franck Daout<sup>b</sup>

<sup>a</sup>Laboratory for Mechanics and Acoustics CNRS, 31 chemin Joseph Aiguier, 13009 Marseille, France

<sup>b</sup>Groupe d'Electromagnétisme Appliqué, Pôle Scientifique et Technologique de l'Université Paris X Nanterre Site de Ville d'Avray, 50, rue de Sèvres, 92410 Paris Ville-d'Avray, France  
herve@lma.cnrs-mrs.fr

Monostatic Synthetic Aperture Sonar (SAS) is a high resolution system which is operational for target imaging purposes in the field of underwater acoustics. The objective of this work was to analyse what kind of information should be obtained from a multistatic SAS system. This idea has been applied in radar but very few works exist in the underwater acoustics domain. The applications could be detection and identification of buried mines or mines lying on the seabed and divers detection for harbour protection. These applications deal with the problem of target detection and identification near a rough interface. To show what can be obtained with a multistatic SAS processing, we have performed an experiment with a circular cylinder and a squared cylinder of  $2a = 1 \text{ cm}$  maximal dimension lying on a rough interface made of sand grains of about 1 mm diameter. Measurements were performed in a tank with both a multistatic and a monostatic forward looking SAS systems. The signal used to insonified the target area was a short impulse with a 2 MHz central frequency which corresponds to a  $ka$  about 40. Images of the cylinder in presence of clutter have been reconstructed with the matched filtering algorithm from monostatic and multistatic acquisitions and were qualitatively compared.

## 1 Introduction

Monostatic Synthetic Aperture Sonar is a high resolution system which is operational for target imaging purposes in the field of underwater acoustics [1]. In the multistatic case, few theoretical or experimental studies have been published [2]. Multistatic SAS is currently increasing attention for use in applications such as the detection and identification of buried mines, mines lying on the seabed or diver detection for harbour protection purposes. In the monostatic configuration, the transmitter and the receiver are located on the same carrier, whereas they are separated in the bistatic configuration. In a multistatic context, combination of various bistatic measurements allows to obtain information of various kinds. Another interesting feature of multistatic configuration is that it allows to choose transducer locations, which makes this kind of configuration highly adaptable and capable of meeting all possible local constraints.

Here, experimental results regarding imaging of targets lying on a rough interface are presented. The imaging algorithm used to reconstruct target images is the Matched Filtering Algorithm (MFA) [3, 4, 5, 6]. In the MFA, the model used to estimate the diffracted field is the ‘‘point scatterers’’ model. Experiment is divided in two parts: target images are reconstructed using a monostatic and then a multistatic forward looking SAS. Two kind of targets were chosen: a circular and a squared cylinders. This study was performed in 2-D to simplify the problem, but the conclusions reached are not restricted to 2-D situations.

In the first part of this paper, geometrical and physical parameters are defined. In a second part, Matched Filtering method adapted to monostatic and multistatic configurations is presented. Then, experimental results in a monostatic and in a multistatic forward looking SAS contexts are presented. Images of circular and squared cylinders were reconstructed with the MFA in both configurations. Lastly, combination of monostatic and multistatic images are presented to put in light the interest of multistatic measurements.

## 2 Geometry and physical parameters

The objective of the study consists in imaging an immersed target (referred to below as  $\Omega_2$ ) lying on a rough interface which was insonified by several transducers

used as transmitters. Waves diffracted by the target were recorded by several transducers used as receivers.  $\Omega_1$  denotes the water which is considered as a free space. The rough interface was not taken into account in the model.  $\Omega_1$  and  $\Omega_2$  are assumed to be homogeneous and isotropic.  $\rho_1$  is defined as the water density and  $c_1$  as the sound velocity in water.  $k_1 = \frac{2\pi f}{c_1}$  denotes the wavenumber in water, where  $f$  is the frequency. This study is performed with two different targets lying on a rough interface and immersed in an experimental tank: a solid circular stainless steel cylinder 1 cm in diameter and a solid squared stainless steel cylinder 1 cm by 1 cm in dimensions. The rough interface was made of sand grains of about 1 mm diameter. Half of the largest dimension of targets (referred to below as  $a$ ).  $p_0(t)$  denotes the time signal transmitted and  $P_0(f)$  denotes its spectrum.

This study is performed in a 2D geometry in order to reduce computational time. ( $Oz$ ) is the symmetry axis of the target. Transducers are placed in the plane ( $xOy$ ). Figure 1 represents a bistatic configuration with a transmitter at T and a receiver at R. Multistatic configuration is defined as a combination of several bistatic configurations.

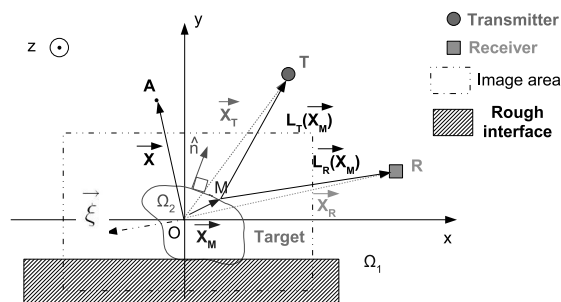


Figure 1: Bistatic configuration

The following vectors are defined:

- $\vec{X} = \vec{OA}$ , where A is any point on the plane ( $xOy$ ) and O is the geometrical center,
- $\vec{X}_T = \vec{OT}$ , where T is the transmitter location,
- $\widehat{X}_T = \frac{\vec{X}_T}{|\vec{X}_T|}$  is the normed vector of  $\vec{X}_T$ ,
- $\vec{X}_R = \vec{OR}$ , where R is the receiver location,

- $\widehat{X}_R = \frac{\vec{X}_R}{|\vec{X}_R|}$  is the normed vector of  $\vec{X}_R$ ,
- $\vec{X}_M = \vec{OM}$ , where M is any point on the target boundary,
- $\hat{n}$  is the outgoing normal from the target boundary,
- $\vec{\xi} = \vec{OP}$ , where P is one of the image pixels.

The following distances are defined:

- $L_T(\vec{X}) = \left| \vec{X}_T - \vec{X} \right|$ ,
- $L_R(\vec{X}) = \left| \vec{X}_R - \vec{X} \right|$ .

The following angles with respect to the  $(O \vec{x})$  axis are defined:

- $(Ox, \vec{X}_T) = \theta_T$ ,
- $(Ox, \vec{X}_R) = \theta_R$ ,

### 3 Imaging Reconstruction Algorithm

Matched Filtering is a well known reconstruction method in the field of Synthetic Aperture Radar [5] and Sonar [6] research. This method has been adapted to bistatic configurations in the case of SAR [5]. It is based on estimation theory and it is the most exact method in the sense of maximum likelihood. A Matched filter is an optimum filter which maximises the signal to noise ratio in the presence of additive stochastic noise.

#### 3.1 Point scatterers model

In this method, the diffracted field is modeled using the “point scatterers” model. The signal received can be written as follows:

$$P^r(\vec{X}_R, k_1) = P^d(\vec{X}_R, k_1) + W(\vec{X}_R, k_1) \quad (1)$$

Where  $P^d(\vec{X}_R, k_1)$  is the field diffracted by the target at R and  $W(\vec{X}_R, k_1)$  is the white circular Gaussian noise at R. The receiver is assumed to do not receive the signal directly transmitted. The model consists in assuming that the target is constituted of  $N$  “point scatterers”.  $\sigma_n$  denotes the reflexion coefficient of the “point scatterer”  $n$  located on the target boundary at point  $M_n$ . The model for the diffracted field is therefore written:

$$P^d(\vec{X}_R, k_1) = \sum_{n=1}^N \sigma_n P_0(f) e^{jk_1 \left[ L_T(\vec{X}_{M_n}) + L_R(\vec{X}_{M_n}) \right]} \quad (2)$$

Where  $\vec{X}_{M_n} = \vec{OM}_n$ .

#### 3.2 Matched filtering algorithm for any geometry

The algorithm is first presented for one transmitter located at T and  $N_R$  receivers located at points  $R_m$ , so that  $m = 1, N_R$ .  $\vec{X}_{R_m} = \vec{OR}_m$  is taken to define  $\widehat{X}_{R_m}$  as the normed vector of  $\vec{X}_{R_m}$  and  $L_{R_m}(\vec{X}) = \left| \vec{X}_{R_m} - \vec{X} \right|$  as the distance between  $R_m$  and any point A on the plane.  $I(\vec{\xi})$  is taken to stand for the intensity of an image pixel located at P. This parameter is the estimator of the maximum likelihood of the reflexion coefficients  $\sigma_n$  based of measurements of  $P^r(\vec{X}_R, k_{1l})$ . The Matched Filtering method is performed on the useful range of frequencies of the transmitted signal spectrum. Frequency values are discretized in  $N_f$  samples. The frequency sample is denoted:  $f_l$ , where  $l = 1, N_f$ , and the wavenumber sample is denoted:  $k_{1l} = \frac{2\pi f_l}{c_1}$ . The Matched Filtered Algorithm (MFA) formula for one transmitter and  $N_R$  receivers is written as follows [5]:

$$I(\vec{\xi}) = \frac{\sum_{m=1}^{N_R} \sum_{l=1}^{N_f} P^r(\vec{X}_{R_m}, k_{1l}) P_0^*(f_l) e^{j\Phi_{l,m}}}{N_R \sum_{l=1}^{N_f} |P_0(f_l)|^2} \quad (3)$$

Where  $P_0^*(f)$  is the conjugate of the transmitted signal spectrum and where  $\vec{\Phi}_{l,m} = k_{1l} \left[ L_T(\vec{\xi}) + L_{R_m}(\vec{\xi}) \right]$ . The image area, in which the target is located, is assumed to be far from the transmitter and receivers. Thus,

- $L_T(\vec{\xi}) = \left| \vec{X}_T - \vec{\xi} \right| \approx \left| \vec{X}_T \right| - \vec{\xi} \cdot \widehat{X}_T$
- $L_{R_m}(\vec{\xi}) = \left| \vec{X}_{R_m} - \vec{\xi} \right| \approx \left| \vec{X}_{R_m} \right| - \vec{\xi} \cdot \widehat{X}_{R_m}$

Hence,

$$I(\vec{\xi}) = \frac{\sum_{m=1}^{N_R} \sum_{l=1}^{N_f} A_{l,m} P^r(\vec{X}_{R_m}, k_{1l}) P_0^*(f_l) e^{-jk_{1l} \cdot \vec{\xi}}}{N_R \sum_{l=1}^{N_f} |P_0(f_l)|^2} \quad (4)$$

Where  $A_{l,m} = e^{jk_{1l} \left[ \left| \vec{X}_T \right| + \left| \vec{X}_{R_m} \right| \right]}$

and with  $k_{l,m} = k_{1l} \left[ \widehat{X}_T + \widehat{X}_{R_m} \right]$ .

The intensity of each pixel results from the correlation between the time signal received; which is denoted  $p^r(\vec{X}_R, t)$ , and a delayed replica of  $p_0(t)$ .

Formula 4 is used to reconstruct an image based on one transmitter and multiple receivers. To obtain the multistatic image based on  $N_T$  transmitters, a coherent sum of these images is performed from 1 to the number of transmitters  $N_T$ .

The monostatic geometry is a particular case of the multistatic one i.e.  $\vec{X}_T = \vec{X}_{R_m} = \vec{X}_{TR_m}$ , where  $\vec{X}_{TR_m}$  denotes the transmission/reception locations, thus:

$$I(\vec{\xi}) = \frac{\sum_{m=1}^{N_{TR}} \sum_{l=1}^{N_f} A_{l,m} P^r(\vec{X}_{TR_m}, k_{1l}) P_0^*(f_l) e^{-jk_{1l} \cdot \vec{\xi}}}{N_{TR} \sum_{l=1}^{N_f} |P_0(f_l)|^2} \quad (5)$$

Where  $A_{l,m} = e^{2jk_{1l}} \left| X_{TR,m}^- \right|$ , with  $k_{l,m}^- = 2k_{1l} \widehat{X_{TR,m}}$  and with  $N_{TR}$  the number of transmission/reception locations.

## 4 Experimental results from a monostatic forward looking SAS

The first experimental study which is presented in this part consists in two monostatic forward looking SAS acquisitions, one at  $40^\circ$  of grazing angle and the other at  $50^\circ$ . Only images performed for  $50^\circ$  of grazing angle will be presented in this part but those performed at  $40^\circ$  will be used in part 6.

### 4.1 Monostatic forward looking SAS acquisition conditions

Figure 2 shows the monostatic forward looking SAS acquisition system. The transducer used in transmission/reception mode was a  $6^\circ$  aperture Imasonic transducer.

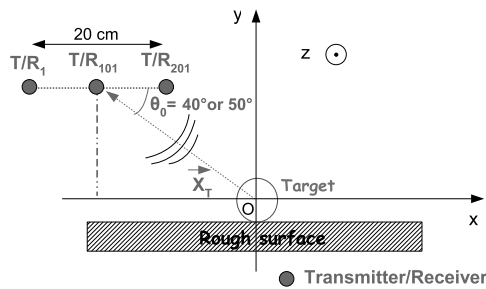


Figure 2: Configuration of the monostatic forward looking SAS

Figure 3 shows the signal filtered by the transducer (left) and its spectrum (right). Its central frequency was  $f_0 = 2 \text{ MHz}$  and the bandwidth at  $-3 \text{ dB}$  was  $720 \text{ kHz}$ . Water density was  $\rho_1 = 1$  and sound speed in the water was approximately  $c_1 = 1480 \text{ m/s}$ , so that  $k_0 a \approx 40$  and  $\lambda_0 \approx 7.10^{-2} \text{ cm}$ .

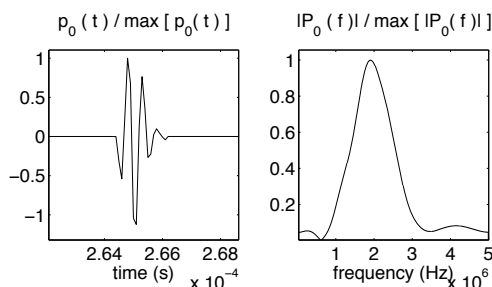


Figure 3: Signal of the monostatic experiment

### 4.2 Circular Cylinder images

Figure 4 shows the image of the circular cylinder lying on the rough interface.

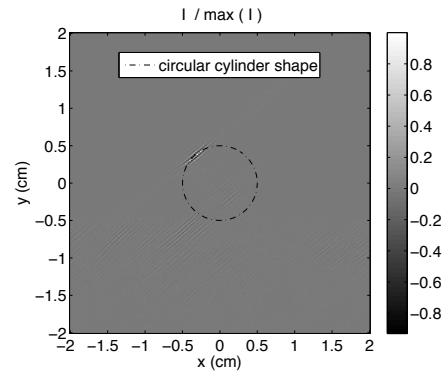


Figure 4: Monostatic image of the circular cylinder

As it can be seen on this image, one “point scatterer” of the circular cylinder was reconstructed and rough interface was also detected. It can be observed the presence of the target shadow behind the target where the rough interface was not reconstructed.

### 4.3 Squared Cylinder images

Figure 5 shows the image of the squared cylinder lying on the rough interface.

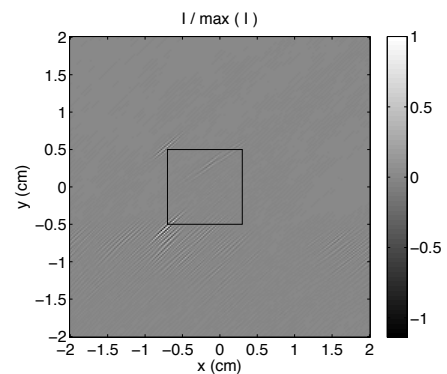


Figure 5: Monostatic image of the squared cylinder

This time two “points scatterer” were reconstructed which defined the two left corners of the squared cylinder. The rough interface was also detected. It can be also observed the presence of the target shadow behind the target where the rough interface was not reconstructed.

## 5 Experimental results from a multistatic forward looking SAS

The second experimental study which is presented in this part consists in two multistatic forward looking SAS acquisitions, one with the transmitter insonifying the target at  $40^\circ$  of grazing angle and the other at  $50^\circ$  using the same reception antenna in the two experiments. The

images performed at  $40^\circ$  and  $50^\circ$  of grazing angles were coherently summed to form one multistatic image.

### 5.1 Multistatic forward looking SAS acquisition conditions

Figure 6 shows the multistatic forward looking SAS acquisition system. The Imasonic transducer used in the monostatic case is taken as the transmitter. An omnidirectional transducer manufactured in the laboratory was used to simulate the reception antenna by moving between two signal acquisitions.

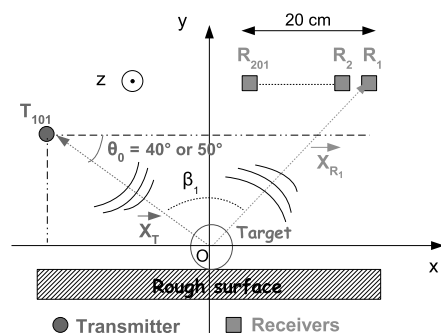


Figure 6: Configuration of the multistatic forward looking SAS

Figure 7 shows the signal filtered by the transmission transducer and the reception transducer (left) and its spectrum (right). Its central frequency was  $f_0 = 2 \text{ MHz}$  and the bandwidth at  $-3 \text{ dB}$  was  $1 \text{ MHz}$ . Water density was  $\rho_1 = 1$  and sound speed in the water was approximately  $c_1 = 1480 \text{ m/s}$ , so that  $k_0 a \approx 40$  and  $\lambda_0 \approx 7.10^{-2} \text{ cm}$ .

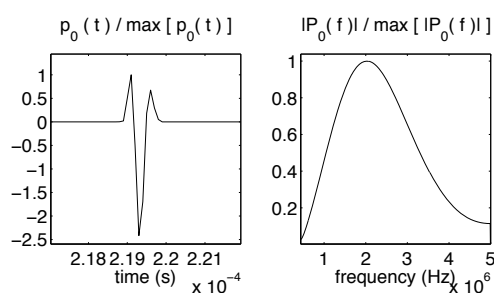


Figure 7: Signal of the multistatic experiment

### 5.2 Circular Cylinder images

Figure 8 shows the image of the circular cylinder lying on the rough interface.

As it can be seen on this image, one “point scatterer” of the circular cylinder was reconstructed and rough interface was also detected. It can be noted that the “point scatterer” reconstructed here is not the same

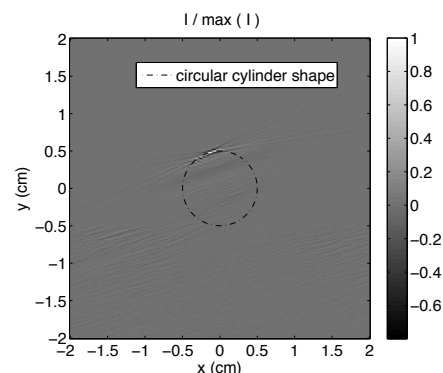


Figure 8: Multistatic image of the circular cylinder

as that reconstructed in the monostatic case. As with the monostatic case, the target shadow is also present in this multistatic image but it is not localized on the same area. Regarding those observations, it can be said that the multistatic image brings different information on the target than the monostatic image.

### 5.3 Squared Cylinder images

Figure 9 shows the image of the squared cylinder lying on the rough interface.

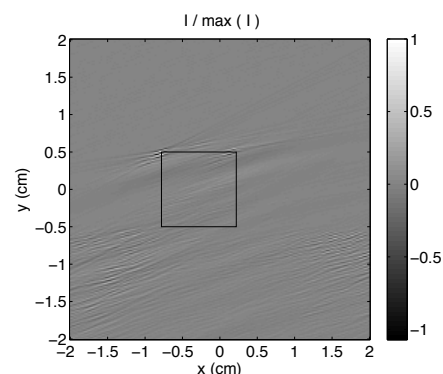


Figure 9: Multistatic image of the squared cylinder

Here, two “points scatterer” were reconstructed which defined the two top corners of the squared cylinder. The rough interface was also detected. Same conclusions as with the circular cylinder can be made. Consequently, monostatic and multistatic images were combined and are presented in the following part, in order to have less uncertainty for target identification purposes.

## 6 Combination of all Experimental results

As monostatic and multistatic images bring different information on targets, coherent sums of all monostatic ( $40^\circ$  and  $50^\circ$  of grazing angle) and multistatic images were performed and are presented in this part.

## 6.1 Circular Cylinder images

The resulting image of the coherent sum of monostatic and multistatic images of the circular cylinder lying on the rough interface is shown figure 10.

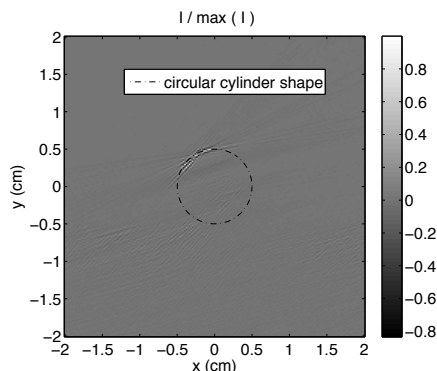


Figure 10: Combination of monostatic and multistatic images of the circular cylinder

It can be seen on this image that the circular cylinder shape is better defined than in previous monostatic or multistatic images.

## 6.2 Squared Cylinder images

The resulting image of the coherent sum of monostatic and multistatic images of the squared cylinder lying on the rough interface is shown figure 11.

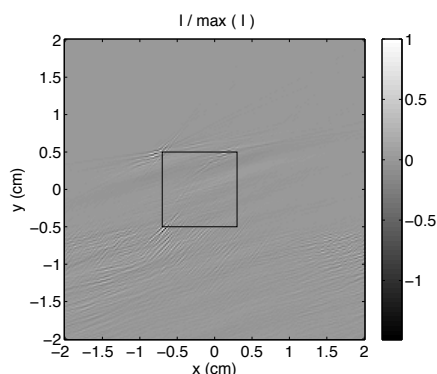


Figure 11: Combination of monostatic and multistatic images of the squared cylinder

It can be seen on this image that three corners of the squared cylinder were reconstructed whereas only two were reconstructed on each monostatic or multistatic images.

## 7 Conclusion

In this paper, images of a circular cylinder and a squared cylinder were reconstructed using the MFA in a monostatic and a multistatic forward looking SAS contexts. First, the two kind of targets were detected on the rough interface. Target shadows on the rough interface were visible with both configurations. From those experiments, it results that this multistatic configuration is interesting for target identification as it allows to see

others "points scatterer" than those visible in the monostatic configuration. Thus, those monostatic and multistatic configurations bring further information that would increase the possibility to identify targets lying on the seabed.

## References

- [1] A. Hetet, "Contribution a la detection de mines enfouies dans le sédiment marin par synthese d'ouverture basse frequence", *Thesis*, University Paris 6, Mechanics (2003)
- [2] J. R. Edwards, H. Schmidt and K. LePage, "Bistatic synthetic aperture target detection and imaging with an AUV", *IEEE Journal of Oceanic Engineering*, 690-699 (2001)
- [3] M. Soumekh, "Synthetic aperture radar signal processing with Matlab algorithms", *Wiley-Interscience*, (1999)
- [4] H. J. Callow, "Signal processing for synthetic aperture sonar image enhancement", *Thesis*, University of Canterbury, Electrical and Electronic of Engineering (2003)
- [5] B. D. Rigling and R. L. Moses, "Polar format algorithm for bistatic SAR", *IEEE*, 1147-1159 (2004)
- [6] P. T. Gough and D. W. Hawkins, "Imaging algorithms for a strip-map synthetic aperture sonar", "Minimizing the effects of aperture errors and aperture undersampling", *IEEE Journal of Oceanic Engineering*, 27-39 (1997)